GNSS measurement of EUV photons flux rate during strong and mid solar flares

M. Hernández-Pajares,[1] A. García-Rigo,[2] J. M. Juan,[1] J. Sanz,[1] E. Monte,[3] and A. Aragón-Àngel[1,2]

Received 6 June 2012; revised 14 October 2012; accepted 18 October 2012; published 12 December 2012.

[1] A new GNSS Solar Flare Activity Indicator (GSFLAI) is presented, given by the gradient of the ionospheric Vertical Total Electron Content (VTEC) rate, in terms of the solar-zenithal angle, measured from a global network of dual-frequency GPS receivers. It is highly correlated with the Extreme Ultraviolet (EUV) photons flux rate at the 26–34 nm spectral band, which is geo-effective in the ionization of the mono-atomic oxygen in the Earth's atmosphere. The results are supported by the comparison of GSFLAI with direct EUV observations provided by SEM instrument of SOHO spacecraft, for all the X-class solar flares occurring between 2001 and 2011 (more than 1000 direct comparisons at the 15 s SEM EUV sampling rate). The GSFLAI sensitivity enables detection of not only extreme X-class flares, but also of variations of one order of magnitude or even smaller (such as for M-class flares). Moreover, an optimal detection algorithm (SISTED), sharing the same physical fundamentals as GSFLAI, is also presented, providing 100% successful detection for all the X-class solar flares during 2000–2006 with registered location outside of the solar limb (i.e., detection of 94% of all of X-class solar-flares) and about 65% for M-class ones. As a final conclusion, GSFLAI is proposed as a new potential proxy of solar EUV photons flux rate for strong and mid solar flares, presenting high sensitivity with high temporal resolution (1 Hz, greater than previous solar EUV irradiance instruments), using existing ground GNSS facilities, and with the potential use as a solar flare detection parameter.

Citation: Hernández-Pajares, M., A. García-Rigo, J. M. Juan, J. Sanz, E. Monte, and A. Aragón-Àngel (2012), GNSS measurement of EUV photons flux rate during strong and mid solar flares, *Space Weather*, *10*, S12001, doi:10.1029/2012SW000826.

1. Motivation

[2] Coinciding with the forthcoming maximum of solar cycle 24, there has been significant growth in the interest in better observation capabilities of the increasing solar flare events, as Space Weather precursors. In particular, higher accuracy and time cadence of the changes within the flux of photons are becoming important to achieve a better understanding of the Sun–Earth interactions (for instance in the new NASA Solar Dynamics Observatory – SDO– EUV Variability Experiment [see *Woods et al.*, 2011]).

[3] So far the main way of obtaining solar flare photon flux measurements has been direct observation from space probes, such as the SOHO and GOES, in EUV and X-ray bands respectively [*Judge et al.*, 1998]. It is also well known that there is a high geo-effectiveness of the radiation in such bands (especially in EUV), which generates photoelectrons in the upper part of the atmosphere, becoming the main source within the ionosphere [see, e.g., *Peterson et al.*, 2009]. In this context the unprecedented increase in temporal and spatial sampling resolutions of the ionosphere by means of the Global Navigation Satellite Systems (GNSS), also in real-time [*Caissy et al.*, 2012], has opened the possibility of indirect solar flare EUV flux rate measurements, being this the main goal of this study.

[4] In this context, the new GPS Solar Flare activity indicator (GSFLAI) is here presented, built from the GPS signature of the ionosphere reaction to the solar flare, i.e., a sudden enhanced ionization, in existing global ground networks. GSFLAI is defined as the VTEC rate gradient in terms of the solar-zenithal angle, and it will be shown that it is fully correlated with the direct EUV spectral measurements, such as those provided by SOHO probe [*Judge et al.*,

[1]Research Group of Astronomy and Geomatics, Universitat Politècnica de Catalunya, Barcelona, Spain.
[2]gAGE-NAV S.L., Barcelona, Spain.
[3]Departament Teoria del Senyal i Comunicacions, Universitat Politècnica de Catalunya, Barcelona, Spain.

Corresponding author: M. Hernández-Pajares, Research Group of Astronomy and Geomatics, Universitat Politècnica de Catalunya, Mod. C3 Campus Nord UPC, Jordi Girona 1-3, ES-08034 Barcelona, Spain. (manuel@ma4.upc.edu)

1998]. The solar flare activity indicator, GSFLAI, can be considered complementary to dedicated solar probes, such as SOHO and GOES (see below), since it provides higher temporal resolution (up to 1 Hz instead of one measurement every 15 s), with no impact on observations by relativistic electrons and no additional costs of exploitation of the existing GPS facilities. Compared with previous works [such as *Afraimovich et al.*, 2002; *García-Rigo et al.*, 2007; *Zhang et al.*, 2011], it will be shown that GSFLAI is a fully quantitative single parameter per time epoch, highly correlated with the solar EUV flux rate, which can be easily computed from the available worldwide distributed GPS receivers. This is also without the need of receivers close to the Earth's sub-solar point (i.e., sun directly overhead), just over the whole daylight hemisphere.

2. Introduction

[5] Solar flares are sudden enhanced electromagnetic emissions, which are often associated with explosive events on the Sun's surface releasing huge amounts of magnetic energy and charged energetic particles. In particular, they are characterized by the emission of radiation across the whole electromagnetic spectrum, especially in X-rays and Extreme Ultraviolet (EUV) band. The radiation in these bands is geo-effective in generating extra photoelectrons in Earth's ionosphere, but affected differently by the locations of flares on the solar disk. X-rays are generally optically thin in the solar atmosphere, therefore are almost unaffected by flare locations. EUV bands are, however, often optically thick in the solar atmosphere. Absorption of optically thick emissions is greater on the limb, due to the longer path lengths. Therefore, limb flares have less enhancement of EUV [*Donnelly*, 1976], and thus are less geo-effective than center flares [*Qian et al.*, 2010]. The radiation photons related to a solar flare facing the Earth produce a sudden enhanced ionization only in the daylight ionosphere that can be approximated by the Chapman model, predicting a dependence on the solar-zenithal angle (SZA or χ; see *Mendillo et al.* [1974] and the next section). Finally, the associated accelerated energetic particles (Solar Energetic Particles SEPs and Energetic Storm Particles ESPs) arrive at the Earth within an interval between 30 min to many hours or even few days later (see *Tsurutani et al.* [2009] for details). Immediately after the arrival of the enhanced photons flux, associated near-relativistic electrons could arrive too, with a median delay of ≃10 minutes [*Haggerty and Roelof*, 2002; see also *Simnett*, 1974]. Note that the energetic particles can enter the Earth through the polar caps and affect the high and middle latitude ionosphere. In such a case, the increase of ionization is not a function of the SZA, and hence does not affect GSFLAI, unlike direct sensors such as the SOHO Solar EUV Monitor.

[6] On the other hand, the GPS constellation of about 30 Medium Earth Orbiting (MEO) satellites, providing ranging signals at two L-band frequencies, has become one of the most successful tools to determine the distribution of free electrons in the ionosphere (see a recent review in *Hernández-Pajares et al.* [2011]). Indeed, GPS, and in general the multifrequency GNSS, provide an unprecedented high spatial and temporal resolution in the measurements of the number of free electrons per volume unit (hereinafter electron density).

[7] In summary, and due to the fact that the X, gamma and especially EUV radiation are responsible for the ionization process in the Earth's ionosphere, it will be shown how the proposed technique takes advantage of this, in order to complement the conventional measurements from space. In this way solar flares can be indirectly but precisely monitored by measuring the electron content enhancement through dual-frequency measurements from a global GPS network.

3. Sudden Enhanced Ionization of the Ionosphere: GSFLAI Model

[8] Due to the short timescale of the impulsive phase of solar flare photon production (typically up to few tens of seconds), it can be assumed that the increase of the electron density in the Earth's ionosphere (and thus its path integral, the TEC) is mainly driven by electron production, rather than loss or migration physical processes. Indeed, following for instance Equation (5) of *Wan et al.* [2002], the variation of the vertical TEC (VTEC), ΔV, for a given solar-zenith angle χ, is proportional to the solar flux increase $\Delta I(t)$ for a given geoeffective spectral range:

$$\frac{\partial V}{\partial t} = \eta' \cdot C(\chi)\Delta I(t) \tag{1}$$

where η' is the corresponding ionization efficiency constant (which will depend on the geo-effectiveness of the considered spectral range). Moreover $C(\chi)$ represents the *cross section* relative to the sub-solar point ($C(0) = 1$) of a differential spherical element of atmosphere in order to generate electron content, which is assumed to be located at the ionospheric effective height, with regard to the Sun illumination at solar-zenithal angle χ. In Figure 1 is a diagram where $C(\chi) \simeq \cos(\chi)$ for $\chi \ll 90$ deg. It will be shown that this simple model performs reasonably well for all values of χ. In this regard, it has to be taken into account that the effective enhanced ionization can be considered located at a certain height of few hundred kilometers above the surface coinciding with the maximum geo-efficiency of solar EUV radiation for molecules such as monoatomic oxygen [*Tobiska*, 2007]. Consequently a certain enhanced ionization for $\chi > 90$ deg can be expected, due to the limb illumination up to $\chi_{\max} = \frac{\pi}{2} + a\cos\left(\frac{R}{R+h}\right)$ (this corresponds for instance to $\chi_{\max} = 104^\circ$ for $h = 200$ km; see Figure 1). This effect is taken into account in the adopted model by

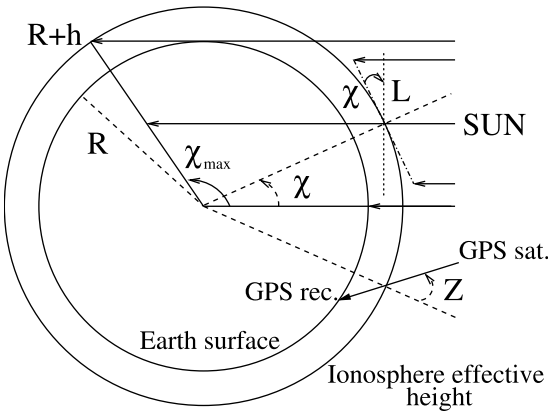

Figure 1. Layout representing the maximum solar-zenith angle illuminated by the Sun, χ_{max}, the reduction of sun illumination for a cylinder with base diameter L for a given solar-zenith angle χ, and the typical satellite receiver geometry for a satellite-zenith angle Z.

including an independent term that allows a non-zero VTEC rate at points with solar-zenith angles $\chi \geq 90^\circ$:

$$\frac{\partial V}{\partial t} = a(t)\cos\chi + b(t) \tag{2}$$

where $a(t)$ is the enhanced ionization gradient for time t and $a(t) + b(t)$ represents the estimated enhanced ionization at the sub-solar point ($\chi = 0$). Both terms, $G_1 \equiv a$ and $G_1 \equiv a + b$, constitute two alternative ways of defining GSFLAI. As will be explained later, G_1 compares slightly better than G_2 with solar EUV flux rate, in such a way that $G \equiv G_1$ will be taken as the baseline definition in the whole paper.

4. Effect in GPS Measurements

[9] The most precise ionospheric observation derived from the dual-frequency GPS phase measurements (L_1 and L_2) is the so-called ionospheric combination of carrier phases (L_I), which provides a direct, precise but ambiguous measurement of slant TEC (STEC), S, with a nominal (thermal noise) measurement error of 0.02 TECU (1 TECU = 10^{16} m^{-2}), which is typically better than 0.1 TECU when the carrier phase multipath error is also considered [see also *Hernández-Pajares et al.*, 2011]. L_I can be expressed in terms of S by means of equation (3):

$$L_I \equiv L_1 - L_2 = \alpha \cdot S + w_I + B_I \tag{3}$$

where $S = \int_{\mathbf{r}}^{\mathbf{r}'} N_e \cdot dl$, α = 0.105 $\cdot$ 10^{-17} m^3 (the scale factor relating the STEC to ionospheric delay for L_I combination), w_I corresponds to the wind-up effect (small, well known and easy to correct for permanent stations), B_I the ambiguity term (which cancels out when considering the observation rate, L_I), N_e is the electron density, and $\mathbf{r}$ and $\mathbf{r}'$ represent the receiver and transmitting satellite positions (see the above mentioned reference for more details).

[10] We are interested in detecting sudden increases of TEC. In this regard, a simple but effective detrending method is to perform consecutive differences in time (for the same satellite-receiver pair) at a high rate (with a sampling rate of 1 Hz). These consecutive time differences at a high rate do not typically increase the observational error due to the low-pass (i.e., low frequency) nature of most of the additive noise present in the signal at 1 Hz (the errors such as multipath are mostly time correlated at such a sampling rate). On the contrary, they can reduce the carrier phase multipath error with variation timescales larger than one second. In this context, such consecutive time differences are able to capture quick solar flux increases associated with solar flares (for larger timescales, larger time periods can be used as well as double-differences in time, as is done for studying Traveling Ionospheric Disturbances for instance in *Hernández-Pajares et al.* [2012]). Moreover, the usage of GSFLAI, as result of the fitting of many VTEC rate values, increases the sensibility of the approach very significantly, with regard to the single difference measurement discussed so far. This is due to its nature as fitting (slope) coefficient, merging many simultaneous observations in the day-hemisphere (ranging between N_{obs} = 47 and 306 from an increasing number of worldwide GPS receivers −25 to 92– between 2001 and 2011 (see for instance Figure 2)). All of these observations have been selected considering a wide distribution in the daylight hemisphere, with a solar-zenithal angle range in dayside hemisphere always greater than 60 deg. and typically larger than 80 deg. This fact augments the sensibility of GSFLAI, G_1, the solar-zenithal gradient of the VTEC rate, a rough factor $\simeq\sqrt{N_{obs}}$, i.e., one order of magnitude greater with regard to STEC rate $\dot{S}$, the input measurement for the fitting, which defines G_1. In other words, the expected error of G_1 is reduced up to about 0.002 TECU/s. This can be appreciated for representative single-epoch examples (see Figures 3 and 4), independently of the solar flare intensity. An additional reduction of the GSFLAI random error is also achieved in this work by smoothing it with a moving average, a sliding window of 15 s (i.e., expected errors down to 0.0005 TECU/s thanks to an extra reduction of a factor of 4 for random errors), in order to be compared with the SOHO-SEM EUV observations, which use this same integration interval.

[11] Moreover, this approach allows the removal of the carrier phase ambiguity (after checking that no cycle-slips have occurred) apart from filtering out the main part of the variability that is not due to the sudden electron content increase. Then, by assuming a simple 2D ionospheric model, for GPS observations taken above a certain elevation cut-off angle (e.g., 15 deg.), the vertical TEC (VTEC) rate, $\dot{V}$, can be easily approximated from equation (3) (GPS model):

$$\dot{V} \equiv \frac{\partial V}{\partial t} \simeq \frac{\Delta V}{\Delta t} \simeq \frac{1}{M}\frac{\Delta S}{\Delta t} = \frac{1}{\alpha M}\frac{\Delta L_I}{\Delta t} \tag{4}$$

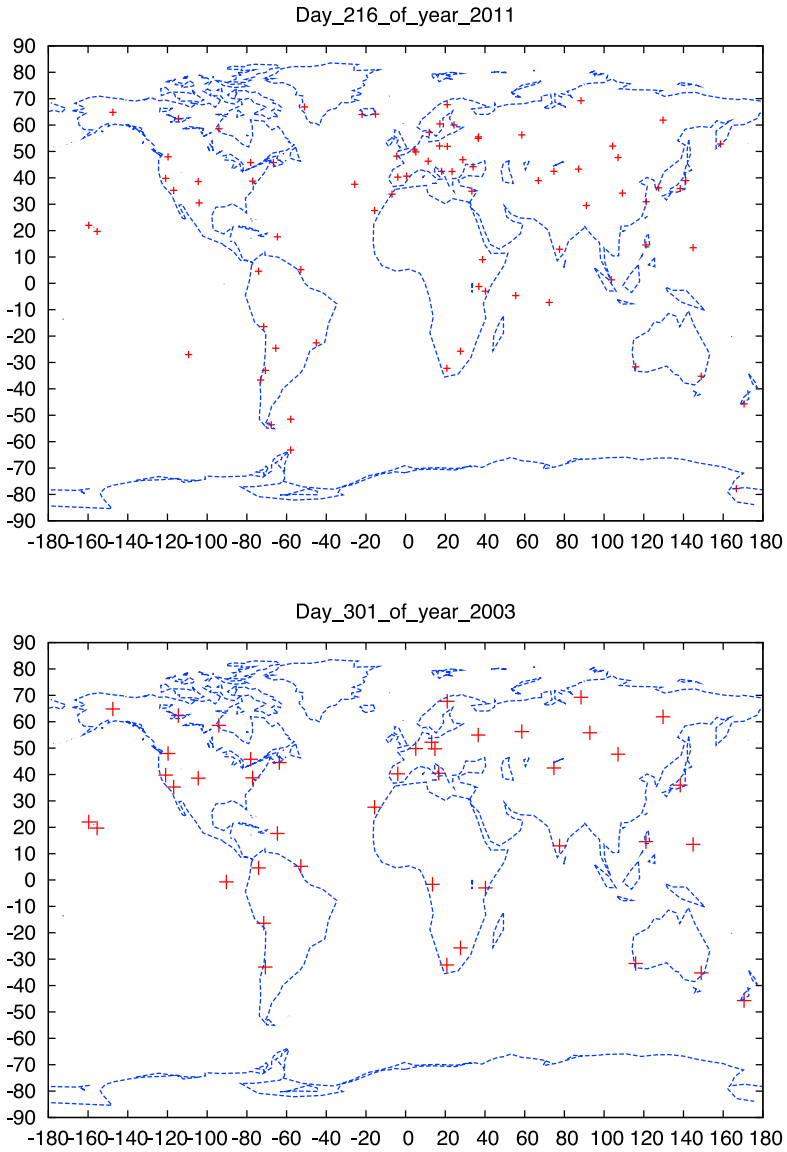

Figure 2. Examples of distribution of selected GPS receivers with available data at 1 Hz for two solar flare events studied in this paper: 80 GPS receivers available for a recent day (216 of year 2011) and 43 for a previous day (corresponding to the Halloween storm precursor), day 301 of year 2003.

where $M \simeq \frac{1}{\cos Z}$ is the deprojection coefficient from vertical to slant TEC, dependent on satellite-zenith angle Z (i.e., on elevation and ionospheric effective height typically taken as 450 km for global VTEC maps [see *Hernández-Pajares et al.*, 2009]), known as "ionospheric mapping function" (see Figure 1 and more details in *Hernández-Pajares et al.* [2011]). From this model and equation (1), our targeted magnitude, the solar flux increase $\Delta I(t)$, can be computed.

5. Input Data: Global GPS Network

[12] The input data are provided by the openly available International GNSS Service (IGS) network of more than 300 dual-frequency GPS receivers (sensitive to the electron content variability by means of equation (3)), distributed worldwide [see *Dow et al.*, 2009], becoming a giant ionospheric sounder of the main affected species: the free electrons [see, e.g., *Hernández-Pajares et al.*, 2011]. The processed subset of IGS receivers (from 25 to 92) has been selected taking one receiver (if any) per each bin of 10 deg. and 5 deg., in longitude and latitude respectively, from the IGS high rate (1 Hz) database (ftp://cddis.gsfc.nasa.gov/highrate). Currently, it can be seen that the number of worldwide available stations, with such spatial resolution, is high enough to increase the accuracy of the proposed approach significantly, bringing the estimated error evolution to less

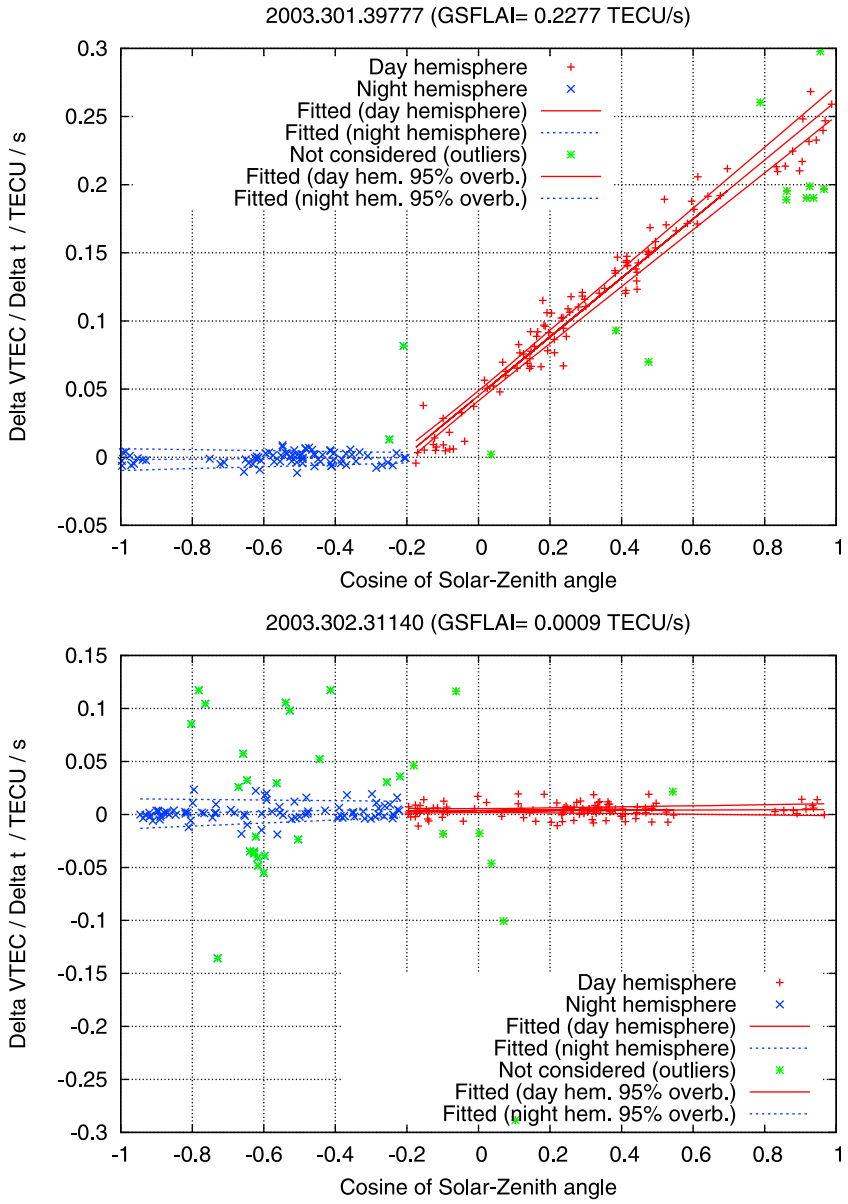

Figure 3. Detrended VTEC rate, $\dot{V}$, vs cosine of solar-zenithal angle, cos χ, for a major solar flare and the associated ionospheric super-storm; from top to bottom: day 301 of 2003, precursor flare of Halloween storm (X17.2 flare, day 301, 2003, 39777 s of GPS time), next day, 302 of 2011 (31140 s of GPS time, when Kp index reach the maximum value of 9). The corresponding regression lines and 2-sigma boundaries are given.

than 0.001 TECU/s, which is consistent with our expectations (see section 4).

[13] Any of the selected receivers directly and simultaneously *observes* the STEC in different line-of-sight directions for several GPS satellites in view. For each satellite-receiver pair a single $\dot{V}$ value can be obtained. As mentioned above, this implies approximately 300 values of $\dot{V}$ calculated at every second for a network (currently available) of about 90 receivers, covering in this way most of the range of values of χ.

6. Reference Data

[14] In order to validate GSFLAI as a potential solar flare activity indicator, two sources of reference data of solar flare events have been considered. On the one hand, the X-ray sensor (XRS) instrument on-board the Geosynchronous

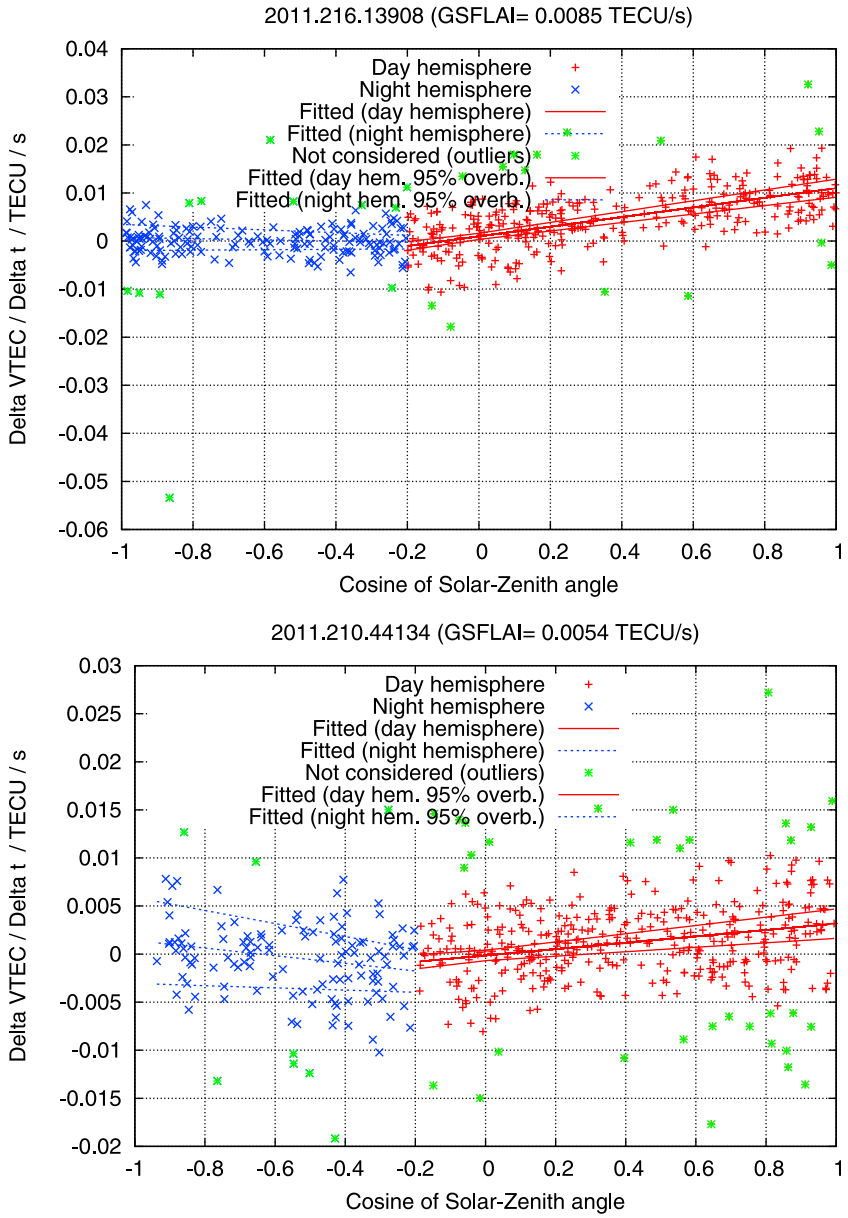

Figure 4. Detrended VTEC rate, $\dot{V}$, vs cosine of solar-zenithal angle, cos χ, for two representative solar flares, with mid and low intensity; from top to bottom: M9.3 flare, day 216 of 2011 (13908 s of GPS time) and C3.9 flare, day 210 of 2011 (44134 s of GPS time). The corresponding regression lines and 2-sigma boundaries are given.

Operational Environmental Satellites (GOES) [*Garcia*, 1994], used for solar flare intensity classification information; and, on the other hand, the Solar EUV Monitor (SEM) on-board the Solar and Heliospheric Observatory (SOHO) (see *Judge et al.* [1998] for details), which has been the main reference data used in this work, for EUV solar flux values. Among the scientific community, the classification of solar flares adopted in the case of GOES XRS is widely accepted, also for EUV photon flux increases in spite of the questioned proportionality relationship between the soft X-flare enhancement and the EUV enhancement during a solar-flare, which can depend on the duration of the flare [*Qian et al.*, 2011]. Ordered from less to more powerful, in powers of 10, several classes named A, B, C, M and X are established according to the peak of intensity in the X-ray band between 0.1 and 0.8 nm. For instance, an *M5* and *X*17.2 flares would have an irradiance of I = 5 * 10^{-5}[W/m^2] and I = 17.2 * 10^{-4}[W/m^2] respectively (further details can be found for instance at

NGDC/NOAA in ftp://ftp.ngdc.noaa.gov). Regarding SEM data, the EUV solar flux measurements provided in the 26–34 nm range are used. This is motivated by both the association with solar active regions of electromagnetic emission in such range, and its previously mentioned absorption in the terrestrial ionosphere, mostly by atomic oxygen above 200 km, the dominant species and source of ionization up to a height of more than 500 km [see *Tobiska*, 2007]. Moreover the usage of such band has the advantage of not becoming saturated in case of extreme solar flare events, which is not the case of larger spectral bands such as the SOHO central channel at 0.1–50 nm. Nevertheless, the 26–34 nm spectral detector performance can be affected by the arrival of Solar Energetic Particles after the solar flare peak [see *Didkovsky et al.*, 2007], as is shown in the next section.

7. Solar Flare Events and Results

[15] In order to illustrate the performance of GSFLAI, two main kinds of results are presented. In section 7.1, and for a representative set of solar flares with different intensities and characteristics, the direct measurements of solar flux rate in EUV are compared with GSFLAI in terms of the time, in order to show that it can become an indirect proxy for such physical magnitude during solar flares (see above). (A time correction is needed to synchronize the SOHO-SEM with the GPS events, both considered at GPS timescale. The SOHO detection appeared to be 20–30 s later (depending on the flare) than that observed through the ionospheric reaction, in the GPS measurements.) In section 7.2 the solar flux EUV excess is directly compared with GSFLAI for all the GOES X-class solar flares that occurred in the period 2001–2011. In section 7.3 a comparison of GSFLAI with GOES X-ray intensity index for X-class events available since 2001 to 2011 is also presented to show that a significant correlation exists for stronger flares, after taking into account the Sun-to-Earth projection factor associated with the point on the Sun surface where the solar flare occurred.

7.1. Representative GSFLAI Examples Under Different Irradiances

[16] A first example in Figure 3 (corresponding to time of precursor X-class flare of Halloween storm at the top, and to the first maximum of geomagnetic activity during the same Halloween storm) illustrates how GSFLAI reacts only to Solar Flares, and is not affected by the corresponding triggered ionospheric storm, in which heterogeneous VTEC variability does not match the enhanced ionization model associated with Solar EUV Flares (equation (2)).

[17] Two additional examples, which are representative of the quality of the simple enhanced ionization model) are shown in Figure 4. The examples correspond to two solar flares peaks of decreasing intensity: M (medium, mid certainty) and C (common, low intensity and with an even more uncertain determination) respectively (every plot is associated with a single GSFLAI number G_1, i.e., its baseline definition as the linear regression slope). The deviations for a few points (marked as outliers and removed) from the ideal linear model are mainly produced by local electron content perturbations and carrier phase measurement errors.

[18] Now the GSFLAI evolution on time will be shown, compared with direct measurements of EUV flux rate. Firstly, once again, one of the greatest solar flare effects ever detected on GPS measurements, from the point of view of TEC increase, was considered. It was recorded on October 28th, 2003 preceding the so-called Halloween storm. This solar flare was classified as X17.2 by GOES, and the VTEC enhancement reached more than 20 TECUs, becoming one of the most widely analyzed in the scientific literature [see, e.g., *Tsurutani et al.*, 2005]. It is shown in Figure 5 (top) that the indirect GSFLAI values and direct EUV rate SOHO SEM measurements correlate well, as do those for the next X flare on November 4th, 2003 (bottom), but with GSFLAI and EUV rate values ten times smaller. An explanation for this discrepancy of one order of magnitude for this case and other very strong solar flares will be presented in section 7.3, in terms of the different geoeffectiveness, when the GOES X-ray classification is considered. Another aspect in the comparisons of GSFLAI versus EUV flux rate, is the tendency for a lower number of negative values to be given in the case of GSFLAI with regard to SEM/EUV flux rate (see for example Figure 5 and Figure 8 (bottom)). In this context, this result is compatible with slower recombination rates in the Earth's ionosphere compared with the preceding sudden enhanced ionization effect.

[19] Another different example is a X7.1 solar flare, reported by GOES on January 20th, 2005. This solar flare is of special interest because of the relativistic electrons that reached the Earth less than 10 min later, which produced a contamination of the SOHO SEM detector providing wrong readings of EUV starting from t = 24750 s of GPS time [see *Tsurutani et al.*, 2009, section 2.3]. However, in Figures 6 (top) and 6 (bottom), it can be seen that GSFLAI remains unaffected due to its definition as solar-zenith angle gradient of VTEC rate (see above) generated by the photons enhancement, since it filters out any influence of relativistic electrons.

[20] Moreover, there is a kind of recently detected solar flare with an important emission at L-band affecting the tracking of the GPS satellites, so, indirectly, they can affect the capability of measuring the solar flare effect in the ionosphere due to the reduction of the number of available electron content measurements. This has happened so far in one case: December 6th, 2006. But even in this case the GSFLAI maintained the high correlation with the direct EUV flux measurement (Figure 6, bottom).

[21] GSFLAI also allows the measurement of many moderate and some common solar flares (class M and C, respectively), being highly consistent as well with direct EUV flux rate measurements for such weaker solar flares. The examples correspond to August 4th and July 29th, 2011, respectively (see Figures 7 (top) and 7 (bottom)).

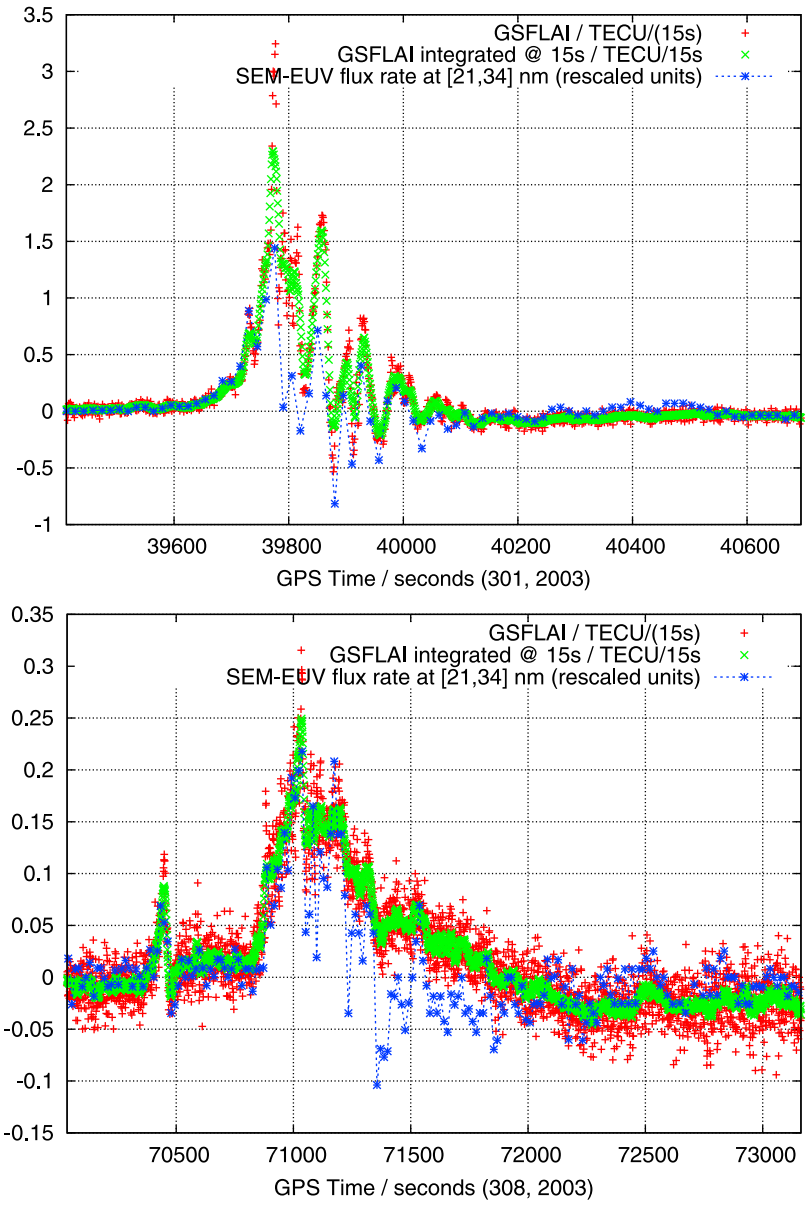

Figure 5. GSFLAI results compared with SEM EUV flux rate at 21-to-34 nm band, $\dot{E}$ provided by SOHO during representative X-class solar flares, and rescaled as $\frac{0.502}{1.5 \cdot 10^8}(\dot{E}/\text{photons/cm}^2/\text{s}^2)$: (top) October 28th, 2003 (X17.2 class); (bottom) November 4th, 2003 (X28.0 class).

7.2. GSFLAI Versus Direct EUV Flux Measurements During X-Class Solar Flares in 2001–2011

[22] When comparing GSFLAI with EUV flux rate, it is remarkable that mainly two conditions are typically fulfilled for different solar flares, in time and intensity, both in agreement with the hypothesis and model (equations (1) and (2); see Figure 8 and Table 1 for all the X-class flares with available SOHO-SEM EUV data within the 2001–2011 period):

[23] (1) There is almost a linear relationship between GSFLAI (computed as the solar-zenithal gradient, and smoothed with a 15-second sliding window), G in TECU/s, and EUV flux rate, $\dot{E}$, in $\text{m}^{-2}\,\text{s}^{-1}$, measured by SOHO-SEM every 15 s.

[24] (2) The slope of the linear dependence appears to some extent repeatable with regard to the solar cycle phase, solar disc location and solar flare intensity: see, for instance in Table 1, the two yearly periods with more comparisons: 2003 in solar maximum and 2011 in solar minimum-middle conditions, where the relationship given between the SOHO SEM EUV rate $\dot{E}$ and GSFLAI G_1 ($\dot{E}$ = 0.502 G_1 + 0.040) can be considered as a first calibration that enables a rough estimate of $\dot{E}$ from G_1.

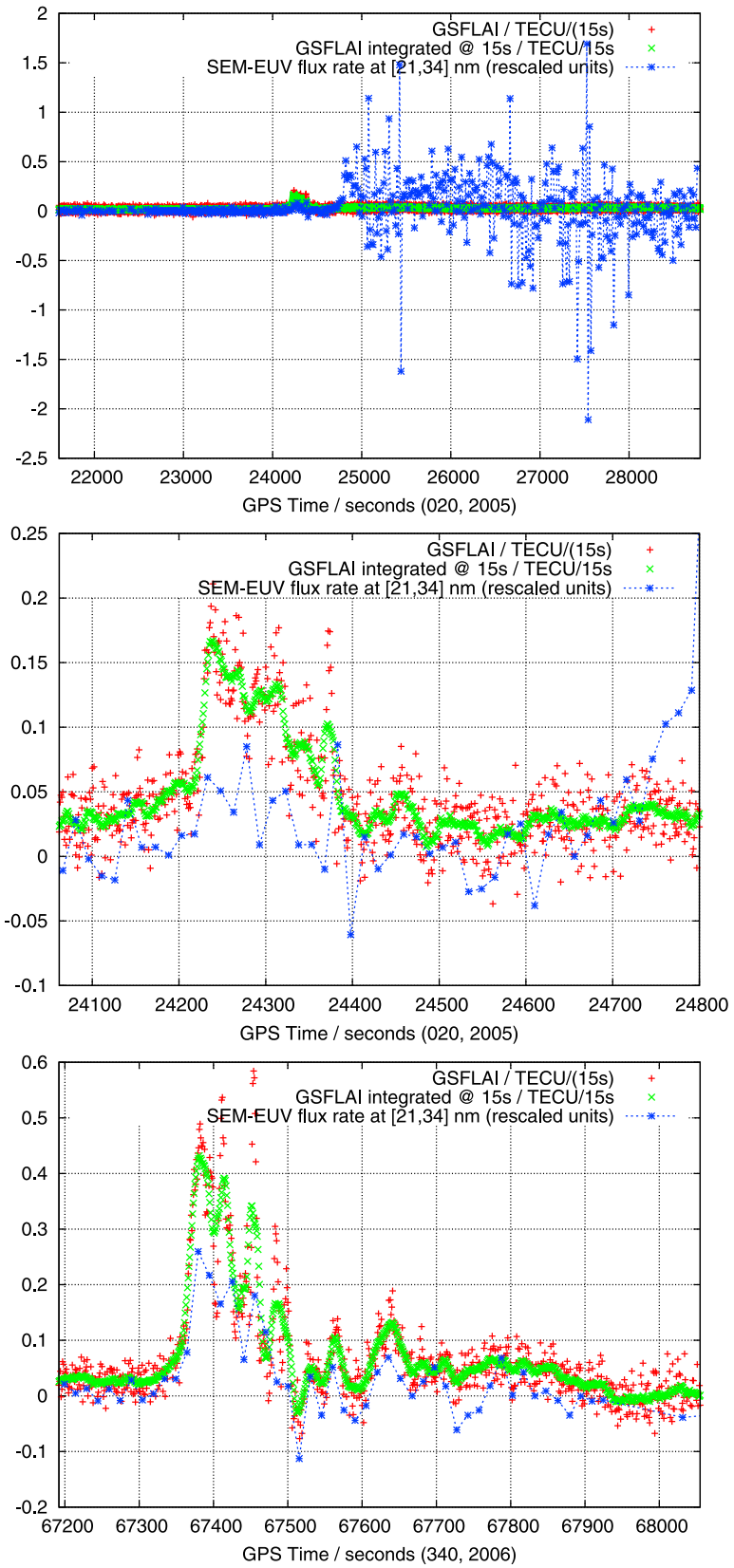
GSFLAI / TECU/(15s)
GSFLAI integrated @ 15s / TECU/15s
SEM-EUV flux rate at [21,34] nm (rescaled units)
GPS Time / seconds (020, 2005)
GSFLAI / TECU/(15s)
GSFLAI integrated @ 15s / TECU/15s
SEM-EUV flux rate at [21,34] nm (rescaled units)
GPS Time / seconds (020, 2005)
GSFLAI / TECU/(15s)
GSFLAI integrated @ 15s / TECU/15s
SEM-EUV flux rate at [21,34] nm (rescaled units)
GPS Time / seconds (340, 2006)

Figure 6

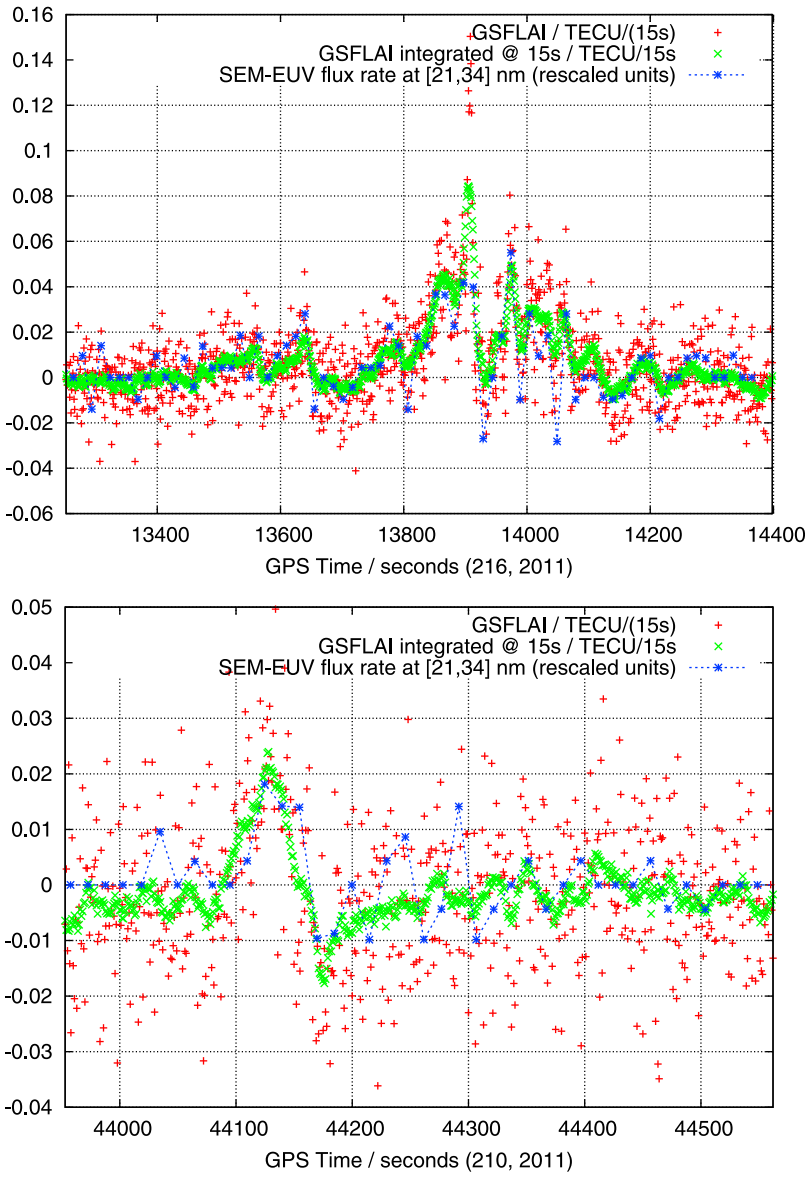

Figure 7. GSFLAI results obtained for (top) August 4th, 2011 and (bottom) July 29th, 2011 (class M9.3 and C3.9 respectively). The comparison with SEM-EUV data is also represented.

[25] And finally, (3), the small observed independent term in the linear fitting of the VTEC rates to the cosinus of solar-zenithal angle is an expected feature considering the initial model and hypothesis. In the future, other strategies could be adopted to further reduce it to avoid a predominant bias term for small flares. (Some potential refinements, that could produce further improvements in future studies, are: adjusting strictly the observations with positive EUV rate only (this reduces the independent term up to 50%) mitigating the effect of a slower recombination at the ionosphere compared with the flare enhanced ionization; or adjusting a higher (second) order model, as an extension of the model represented in equation (2) (this independent term has been avoided in the rescaled EUV flux rate for the comparisons versus time shown in Figures 5, 6, and 7).)

Figure 6. Same plots as the Figure 5 but for the following X-class solar flares of photons: January 20th, 2005 (X7.1 class), showing (top) a general evolution and (middle) a zoom and (bottom) December 5th, 2006 (X6.5 class).

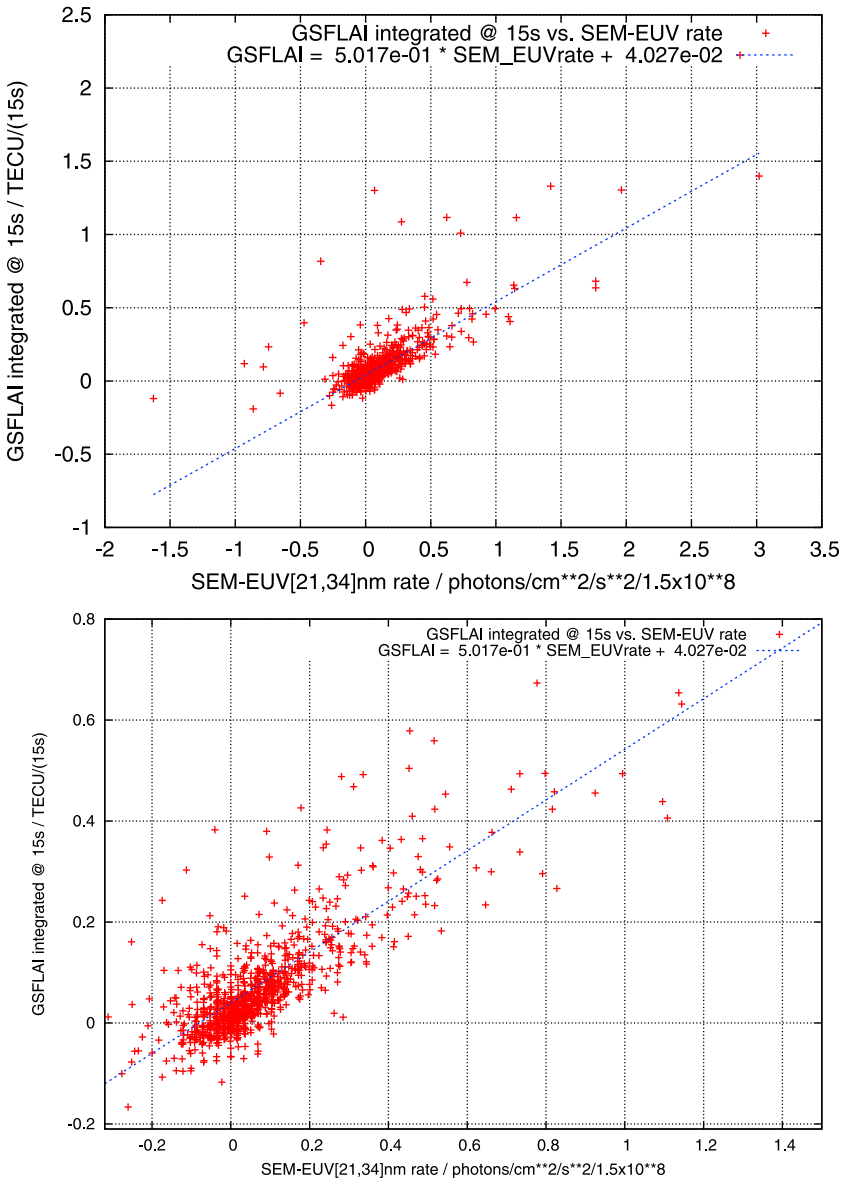

Figure 8. (top) GSFLAI versus direct EUV rate measurement (SOHO SEM) in 26–34 nm spectral band, for all the X-class solar flares with available SOHO-SEM data within 2001–2011. (bottom) A zoomed view. The common linear fit in the corresponding units is also represented as reference (G/TECU/15 s) = 0.502 $\cdot$ 10^{-8}($\dot{E}$/photons/cm^2/s^2)/1.5 $\times$ 10^8 + 0.040).

[26] Moreover, a slightly better fitting of G_1 with the EUV flux rate has been found in this study, rather than of the second definition G_2 (the estimated $\dot{V}$ at the sub-solar point; shown also in section 3), which justified the main definition of GSFLAI as the solar-zenithal gradient of $\dot{V}$.

7.3. GSFLAI Versus X-Ray GOES Intensity at X-Class Solar Flare Peaks

[27] As has been commented above, and following *Donnelly* [1976], the X-ray flux reaching the Earth is not affected by solar atmospheric absorption, compared with EUV flux that is highly dependent on the flare location distance to the solar disc center. In this section this point will be checked. This allows an extension of the definition of GSFLAI, corrected by the solar disc location of the flare in a simple way, in order to provide a geophysically consistent parameter.

[28] In Figure 9, the one-to-one global GPS and GOES data comparison can be seen for all the X-flares occurring in the same period of 2001–2011, when both kinds of data were available (a total of 61 X-class solar flares). It can be

Table 1. Linear Fitting Coefficients of GSFLAI Versus SOHO SEM EUV Solar Flux Rate Computed Independently for Each Year With Available X-Class Flares Within 2001–2011[a]

Year	Number of Points	*G* Slope (TECU/15 s)	*G* Ind. Term (TECU/15 s)
2001	125	0.472 ± 0.027(5.7%)	0.055 ± 0.007(12%)
2002	41	0.421 ± 0.016(3.7%)	0.025 ± 0.010(41%)
2003	364	0.517 ± 0.026(5.0%)	0.056 ± 0.008(15%)
2004	37	0.269 ± 0.031(11%)	0.036 ± 0.002(5.2%)
2005	140	0.689 ± 0.047(6.8%)	0.026 ± 0.007(26%)
2006	114	0.591 ± 0.033(5.6%)	0.038 ± 0.005(12%)
2011	264	0.531 ± 0.021(3.9%)	0.019 ± 0.002(11%)
All	1085	0.502 ± 0.013(2.5%)	0.040 ± 0.003(8.0%)

[a]G value is smoothed with the 15-s SOHO-SEM integration time. During years 2007 to 2010 no X-class solar flares occurred. The units are TECU/15 s for GSFLAI and photons/cm^2/s^2/1.5 · 10^8 for SEM-EUV flux rate at [21–34] nm range.

seen that a much more linear relationship appears, mainly for stronger flares, when the solar flare location at the Sun's surface is taken into account in such a way that a projection factor toward the Sun-to-Earth direction is applied to X-flux data, resembling EUV flux absorption on the solar disc (see above). In particular, this enables understanding of the small ionospheric reaction to the stronger X-flare on November 4th, 2003 (already shown in Figure 5) in terms of a very poor geo-effectiveness, that occurred very close to the west border of the Sun, as it was seen from the Earth.

7.4. Solar Flare Detection: SISTED

[29] In this work GSFLAI is complemented with a new associated detection algorithm, the Sunlit Ionosphere Sudden TEC Enhancement Detector (SISTED), based on the same physical foundations. It shows reliable detection performance of 94% of X-class solar flares during more than half solar cycle (and 65% for M-class flares). In order to set up a real-time operational system to study solar flares, it is necessary to design and implement an efficient detector, companion of the solar flare EUV photon flux rate proxy, GSFLAI. In this regard, the new SISTED has been developed by the authors, based on similar fundamentals, and on an evolution of a previous detector [*García-Rigo et al.*, 2008]. The first distinction is the usage of the VTEC drift rate $\ddot{V}$ (instead of just the rate as in GSFLAI) for a better TEC detrending, due to its typical application to GPS data sampled at 1/30 Hz (instead of each second) in real-time applications. Then, the output values are classified according to the SZA that is given at the corresponding Ionospheric Pierce Point (IPP) location (initially assuming a thin single layer ionospheric model at a given fixed height, for instance 450 km). Three SZA regions are distinguished as an approximation of: (1) the sunlit ionosphere region ($SZA < 70°$), (2) the dawn and dusk ionosphere region ($70° \le SZA \le 110°$) and (3) the night-side ionosphere region ($SZA > 110°$). At each epoch, the percentage of GPS rays that are simultaneously affected by a sudden TEC enhancement for a given threshold is calculated for each of the SZA regions. These percentages are named Impact

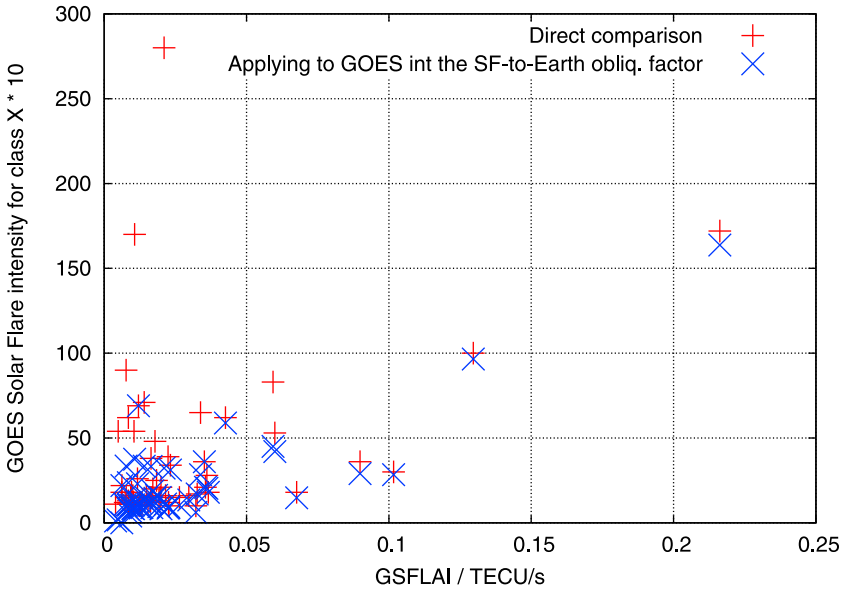

Figure 9. X-ray band solar flare intensity, corresponding to the GOES index for all the X-class flares analyzed in this work (those with available data between 2001 and 2011) represented versus the GSFLAI value at the corresponding peak. The red points represent the direct comparison, and the blue points the comparison after applying a solar-earth deprojecting factor, in terms of the solar flare occurrence location in the surface of the Sun.

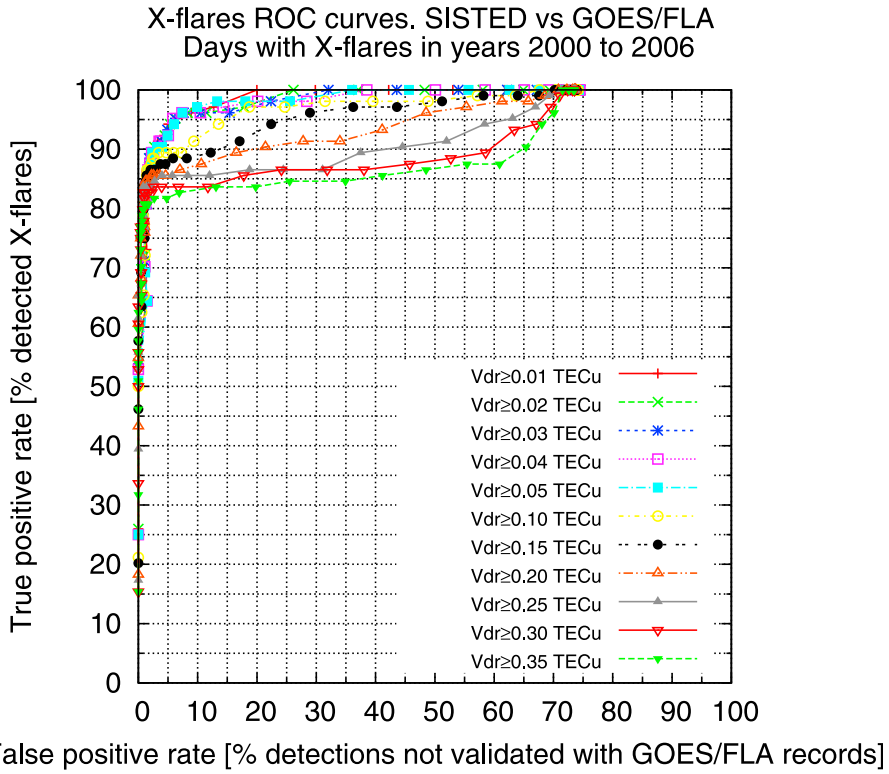
X-flares ROC curves. SISTED vs GOES/FLA
Days with X-flares in years 2000 to 2006
True positive rate [% detected X-flares]
False positive rate [% detections not validated with GOES/FLA records]
Vdr≥0.01 TECu
Vdr≥0.02 TECu
Vdr≥0.03 TECu
Vdr≥0.04 TECu
Vdr≥0.05 TECu
Vdr≥0.10 TECu
Vdr≥0.15 TECu
Vdr≥0.20 TECu
Vdr≥0.25 TECu
Vdr≥0.30 TECu
Vdr≥0.35 TECu

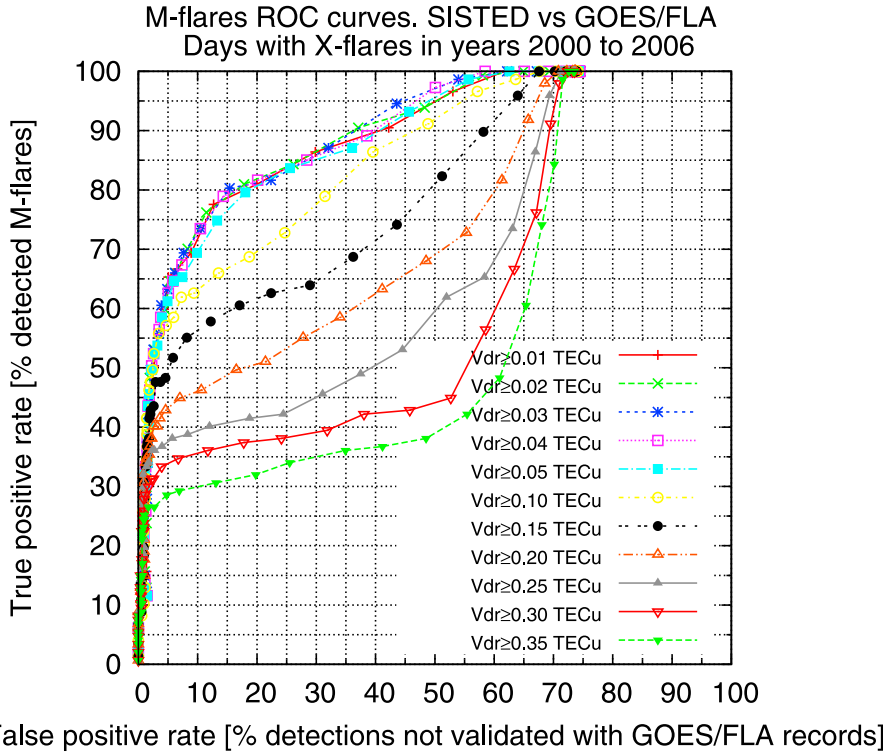
M-flares ROC curves. SISTED vs GOES/FLA
Days with X-flares in years 2000 to 2006
True positive rate [% detected M-flares]
False positive rate [% detections not validated with GOES/FLA records]
Vdr≥0.01 TECu
Vdr≥0.02 TECu
Vdr≥0.03 TECu
Vdr≥0.04 TECu
Vdr≥0.05 TECu
Vdr≥0.10 TECu
Vdr≥0.15 TECu
Vdr≥0.20 TECu
Vdr≥0.25 TECu
Vdr≥0.30 TECu
Vdr≥0.35 TECu

Figure 10

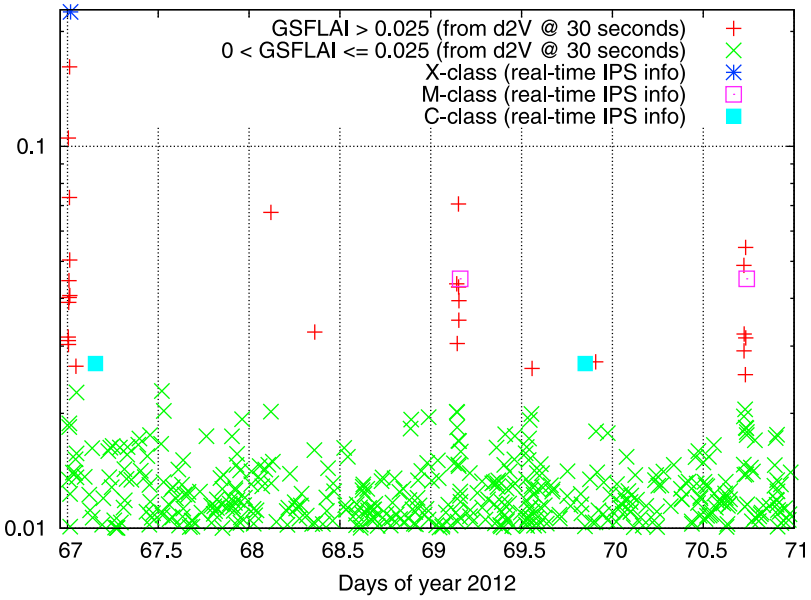

Figure 11. Example of recent values of GSFLAI computed in real-time at 30 second interval, based on double-time difference. The values higher than 0.025 m are highlighted and compared with the real-time IPS warning of solar flares. It can be seen as the X-class flare and the two M-class flares occurring during these four consecutive days were detected in real-time, coinciding with the real-time warnings. This is not the case for the weaker C-class, as was to be expected.

parameters (referred to as $I_1/I_2/I_3$ for the sunlit/dawn&-dusk/night ionosphere regions). In this context, the $\ddot{V}$ threshold to consider a sudden enhanced ionization is slightly above the level of measurement noise of L_I (see Figure 10 and associated comments), taking into account (see equation (4)) that $(\Delta t)^2 \cdot \ddot{V} \simeq -2(V - \hat{V}) \simeq -2M^{-1}(L_I - L_I)$, where V and L_I are the central values of the three involved in the double difference in time, and $\hat{V}$ and L_I are the corresponding means of the two extreme values for V and L_I. A solar flare warning is triggered when, for instance, $\ddot{V} \geq 0.01$ TECU/30 s, and when $I_1 \geq 72\%$, so most GPS rays in the sunlit region must be affected by a sudden TEC increase. In short, there are two filters acting collaboratively: the filter to declare the individual TEC rate measurement as "disturbed", and the second one given by the degree of the "global disturbance" in terms of solar-zenithal sectors. Note that the contribution caused by other sources, such as TIDs or Scintillations, is filtered out, similarly to GSFLAI, due to the solar-zenithal dependence sought in the above defined ratios, and even, in the case of TIDs, due to the implicit filtering in the individual VTEC double differences, taken at 30-second intervals (too small when compared with the targeted TID periods of many hundreds of seconds [see, e.g., *Hernández-Pajares et al.*, 2012]).

[30] The obtained results for more than half solar cycle show that SISTED can detect, in particular, 94% of the powerful solar flares detected by GOES (X-class) between 2000 and 2006 corresponding to a 5% of false positive detections, following the GOES records. It is important to note that the remaining 6% of undetected powerful flares correspond to occurrences in the solar disc limb with much less geo-effectiveness (see previous section) or few cases without location information. This performance as a function of the detection threshold is summarized by using the "Receiver Operating Characteristic" (ROC) curve. The ROC curves of our SISTED detector are depicted in Figure 10, representing the true positive detection rate versus the false positive rate, for different curves given by different $\ddot{V}$ thresholds, and different sunlit impact parameters (points on a given curve).

Figure 10. SISTED ROC curves representing the true positive rate of solar flare detection (percentage of flares validated with GOES/FLA records) versus the false positive rate, for (top) X-class flares (percentage of reported flares not validated) and (bottom) M-class flares, during the days with X-class flares detected by GOES between years 2000 and 2006. Each curve corresponds to a different threshold when considering the measurement "perturbed" ($\ddot{V} \equiv$ "Vdr" in the plot legend) and it is built taking into account steps of 2% of the minimum value of the sunlit Impact Parameter (ranging from 0% to 100%) for each given curve.

[31] These results provided by SISTED, an algorithm designed for solar flare detection directly related with the solar flare activity indicator GSFLAI, suggest the potential future usage of GSFLAI in order to become a simple solar flare detector. Indeed, a first glance can be seen in Figure 11. This recent example shows the comparison of the GSFLAI values computed recently in actual real-time conditions, G_1^*, from data of the International GNSS Real-Time Service network [*Caissy et al.*, 2012], against the real-time solar flare warnings provided by the Ionospheric Prediction Service (IPS, http://www.ips.gov.au/). (In order to speed up the process, the VTEC drift rate computed every 30-seconds (instead of the VTEC rate each second) is adjusted against the solar-zenith angle.) This run of 4 consecutive days illustrates their typical consistency, not only for X-class but also for M-class flares, when the 99-percentile of the G_1^* values in the years 2010–2011 ($\simeq$0.025 m) is taken into account (red points) as a preliminary detection threshold.

8. Conclusions

[32] In this paper, it has been shown that the solar-zenithal gradient of the ionospheric electron content increase (GSFLAI), measured from a global network of GPS receivers, is an efficient and accurate high rate proxy of EUV photons flux increase during strong and mid solar flares. Beyond the higher temporal resolution (1 Hz), GSFLAI has other advantages complementing the usage of space probe measurements of EUV rate: GSFLAI is not contaminated by the ejection of rapid particles from the Sun, and there is no need for extra investment to have a continuous monitoring thanks to the existing permanent global GPS network. Moreover, GSFLAI clearly appears to be also related, for the stronger solar flares, with the X-ray GOES intensity when the Sun-to-Earth deprojection factor is applied, from the solar flare location on the Sun's surface, being consistent with the different geoeffectiveness properties of X-ray and EUV enhanced flux, as pointed out in the above mentioned works. Another aspect also evidenced in this work is the expected slower recombination at the ionosphere, compared with its corresponding sudden enhanced ionization.

[33] Apart from that, it has also been shown that a specific solar flare detector (SISTED), based on the same physical foundation, performs well, detecting all the X-class flares with know location outside the solar limb (94% of the total), and 65% for M-class flares, during more than half solar cycle. And the first encouraging results of the usage of the same GSFLAI parameter as solar flare detector, running in actual real-time conditions, have also been shown.

[34] **Acknowledgments.** This work was partially supported by the projects CTM2010-21312-C03-02 and TEC2009-14094-C04-01 (Spanish Ministry of Science and Innovation), and it was done coinciding with the MONITOR activity (ESTEC-ESA) for the first real-time runs of GSFLAI as detector. The ground GPS data was obtained from IGS permanent and real-time networks, the COSMIC measurements have been obtained from UCAR and TAC, and the SOHO data and Edited Solar Events List from NGDC/NOAA.

References

Afraimovich, E. L., A. T. Altynsev, V. V. Grechnev, and L. A. Leonovich (2002), The response of the ionosphere to faint and bright solar flares as deduced from global GPS network data, *Ann. Geophys.*, *45*(1), 31–40.

Caissy, M., L. Agrotis, G. Weber, M. Hernandez-Pajares, and U. Hugentobler (2012), The International GNSS Real-Time Service, report, GPS World, Santa Ana, Calif., June.

Didkovsky, L. V., D. L. Judge, A. R. Jones, S. Wieman, B. T. Tsurutani, and D. McMullin (2007), Correction of SOHO CELIAS/SEM EUV measurements saturated by extreme solar flare events, *Astron. Nachr.*, *328*(1), 36–40, doi:10.1002/asna.200610667.

Donnelly, R. F. (1976), Empirical models of solar flare X ray and EUV emission for use in studying their *E* and *F* region effects, *J. Geophys. Res.*, *81*(25), 4745–4753.

Dow, J., R. Neilan, and C. Rizos (2009), The international GNSS service in a changing landscape of global navigation satellite systems, *J. Geod.*, *83*(3–4), 191–198, doi:10.1007/s00190-008-0300-3.

Garcia, H. A. (1994), Temperature and emission measure from goes soft X-ray measurements, *Sol. Phys.*, *154*(2), 275–308.

García-Rigo, A., M. Hernández-Pajares, J. M. Juan, J. Sanz (2007), Solar flare detection system based on global positioning system data: First results, *Adv. Space Res.*, *39*, 889–895.

García-Rigo, A., M. Hernández-Pajares, J. M. Juan, and J. Sanz (2008), Real time ionospheric TEC monitoring method applied to detect solar flares, *Geophys. Res. Abstr.*, *10*, EGU2008-A-09358.

Haggerty, D. K., and E. C. Roelof (2002), Impulsive near-relativistic solar electron events: Delayed injection with respect to solar electromagnetic emission, *Astrophys. J.*, *579*, 841–853.

Hernández-Pajares, M., J. M. Juan, J. Sanz, A. Garcia-Rigo, J. Feltens, A. Komjathy, S. C. Schaer, and A. Krankowski (2009), The IGS VTEC maps: A reliable source of ionospheic information since 1998, *J. Geod.*, *83*(3–4), 263–275.

Hernández-Pajares, M., J. M. Juan, J. Sanz, A. Aragón-Àngel, A. García-Rigo, D. Salazar, and M. Escudero (2011), The ionosphere: Effects, GPS modeling and the benefits for space geodetic techniques, *J. Geod.*, *85*, 887–907, doi:10.1007/s00190-011-0508-5.

Hernández-Pajares, M., J. M. Juan, J. Sanz, and A. Aragón-Àngel (2012), Propagation of medium scale traveling ionospheric disturbances at different latitudes and solar cycle conditions, *Radio Sci.*, *47*, RS0K05, doi:10.1029/2011RS004951.

Judge, D. L., et al. (1998), First solar EUV irradiances obtained from SOHO by the Celias/Sem, *Sol. Phys.*, *177*(1–2), 161–173.

Mendillo, M., et al. (1974), Behavior of the ionospheric *F* region during the Great Solar Flare of August 7, 1972, *J. Geophys. Res.*, *79*(4), 665–672.

Peterson, W. K., E. N. Stavros, P. G. Richards, P. C. Chamberlin, T. N. Woods, S. M. Bailey, and S. C. Solomon (2009), Photoelectrons as a tool to evaluate spectral variations in solar EUV irradiance over solar cycle timescales, *J. Geophys. Res.*, *114*, A10304, doi:10.1029/2009JA014362.

Qian, L., A. G. Burns, P. C. Chamberlin, and S. C. Solomon (2010), Flare location on the solar disk: Modeling the thermosphere and ionosphere response, *J. Geophys. Res.*, *115*, A09311, doi:10.1029/2009JA015225.

Qian, L., A. G. Burns, P. C. Chamberlin, and S. C. Solomon (2011), Variability of thermosphere and ionosphere responses to solar flares, *J. Geophys. Res.*, *116*, A10309, doi:10.1029/2011JA016777.

Simnett, G. M. (1974), Relativistic electron events in interplanetary space, *Space Sci. Rev.*, *16*(1-2), 257–323.

Tobiska, W. K. (2007), SOLAR2000 v2.30 and SOLARFLARE v1.01: New capabilities for space system operations, paper AIAA-2007-0495 presented at 45th AIAA Aerospace Sciences Meeting and Exhibit, Am. Inst. of Aeronaut. and Astronaut., Reno, Nev., 8–11 Jan.

Tsurutani, B. T., et al. (2005), The October 28, 2003 extreme EUV solar flare and resultant extreme ionospheric effects: Comparison to other Halloween events and the Bastille Day event, *Geophys. Res. Lett.*, *32*, L03S09, doi:10.1029/2004GL021475.

Tsurutani, B. T., O. P. Verkhoglyadova, A. J. Mannucci, G. S. Lakhina, G. Li, and G. P. Zank (2009), A brief review of "solar flare effects" on the ionosphere, *Radio Sci.*, *44*, RS0A17, doi:10.1029/2008RS004029. [Printed *45*(1), 2010.]

Wan, W., H. Yuan, L. Liu, and B. Ning (2002), The sudden increase in ionospheric total electron content caused by the very intense solar flare on July 14, 2000, *Sci. China Ser. A*, *45*(1), 142–147.

Woods, T. N., et al. (2011), New solar extreme-ultraviolet irradiance observations during flares, *Astrophys. J.*, *739*, 59, doi:10.1088/0004-637X/739/2/59.

Zhang, D. H., X. H. Mo, L. Cai, W. Zhang, M. Feng, Y. Q. Hao, and Z. Xiao (2011), Impact factor for the ionospheric total electron content response to solar flare irradiation, *J. Geophys. Res.*, *116*, A04311, doi:10.1029/2010JA016089.